Effect of channel asymmetry on the behavior of flow passing through the glottis

Kaburagi, Tokihiko
Faculty of Design, Kyushu University

出版情報：Acoustical Science and Technology. 33 (6), pp.348-358, 2012. 日本音響学会
バージョン：

Acoust. Sci. & Tech. **33**, 6 (2012)

PAPER

Effect of channel asymmetry on the behavior of flow passing through the glottis

Tokihiko Kaburagi*

Faculty of Design, Kyushu University,
4–9–1 Shiobaru, Minami-ku, Fukuoka, 815–8540 Japan

(*Received 13 February 2012, Accepted for publication 9 May 2012*)

Abstract: A method for analyzing the behavior of flow passing through an asymmetrical glottal channel is presented. The method assumes the formation of a thin boundary layer near the glottal wall and an interaction between the boundary layer and the core flow. The core flow velocity is estimated in two dimensions employing a method of potential flow analysis, while the characteristic quantities of the boundary layer are determined by solving the integral momentum relation on the basis of the similarity of the velocity profiles within the layer. Estimation results for the volume flow rate, effective flow velocity, pressure distribution, driving force of the vocal folds, and flow separation point are presented for a total of 315 glottal configurations obtained by varying the angle of each vocal fold and the minimum glottal height. The results indicate that the boundary layer tends to reduce the effect of channel asymmetry, and the imbalance of the aerodynamic quantities between the two vocal folds is small unless the glottis widely opens and the angular difference of the vocal folds is considerable.

Keywords: Voice production, Glottal flow, Asymmetrical channel, Boundary-layer analysis

PACS number: 43.70.Aj [doi:10.1250/ast.33.348]

1. INTRODUCTION

The sound source of voice is generated through mutual interactions of physical processes, namely, the aerodynamic behavior of flow passing through the glottis, viscoelastic motion of the vocal folds, and acoustic pressure in the vicinity of the glottis arising from the acoustic characteristics of the vocal tract [1–3]. Vibration of the left and right vocal folds is regular and synchronous in normal phonation. If the vocal fold motion becomes irregular, the generated voice source entails hoarseness. Irregular vocal fold motion and pathological voices have been studied using the coupled mass-spring model of the vocal fold [4–8], typically having two degrees of freedom for each fold. By changing the natural frequency of the left and right folds independently, the possible cause of irregular vocal fold motion and a hoarse voice was investigated in relation to the tension imbalance of the vocal folds or unilateral mass increase. In particular, Steinecke and Herzel [6] applied the theory of nonlinear dynamics and presented precise bifurcation diagrams with respect to the parameters of the vocal fold model.

Prediction of irregular, asymmetrical motion of the vocal folds has been extensively investigated, but less attention has been paid to the analysis of glottal flow for the pathological voice. The behavior of the vocal folds determines the configuration of the glottal aperture. At the same time, the dynamic behavior of glottal flow is largely dependent on the glottal shape. In regular phonation, the glottal shape is convergent during the opening phase of the glottal cycle and divergent during the closing phase [2]. The aerodynamic pressure of glottal flow then becomes both positive and negative according to the convergent–divergent change in the glottal shape, supporting the maintenance of the vocal fold oscillation [9–11]. As such, precise analysis of flow behavior will increase our knowledge about the mechanism of voice production for both the regular case and irregular pathological case.

For simplicity, the flow behavior is usually assumed as being one-dimensional [2,4–9]. By assuming that the flow is steady and incompressible, Bernoulli's law is applied to determine the relationship between the flow velocity and the pressure distribution along the glottal wall. This analysis method is reliable if the friction loss due to the air viscosity and estimation of the flow separation point are incorporated [9,10]. In the case of the pathological voice, however, the glottal channel is asymmetrical because of unbalanced motion of the left and right vocal

*e-mail: kabu@design.kyushu-u.ac.jp

folds. Therefore, the glottal flow should, at least, be regarded as two-dimensional, but it makes the numerical analysis much more difficult.

A number of examinations have been performed thus far focusing on the analysis of the asymmetrical behavior of the glottal flow. Tao *et al.* [12], for example, numerically solved the Navier-Stokes equations to show the occurrence of the Coanda effect in the symmetrical glottis. A similar computational fluid dynamics approach was used for both symmetrical and asymmetrical glottal channels [13,14]. On the other hand, it has been revealed that the analysis methods based on the boundary-layer approximation are highly accurate and computationally efficient [9–11,15]. Lagrée *et al.* [16] applied a method called interactive boundary-layer (IBL) analysis to investigate the asymmetrical effects, and they calculated the distribution of the characteristic quantities of glottal flow along the channel. However, the analysis was performed only for a simplified channel shape. Kalse *et al.* [17] also presented the theory of IBL analysis, but a complete analysis procedure was not presented for the case of two-dimensional flow.

By extending our previous flow analysis studies [10,11], this paper presents a method for analyzing the two-dimensional flow in asymmetrical glottal channels. In addition to the boundary-layer approximation, our method considers the coupling between the main flow, which is assumed to be inviscid, and the boundary layer, which is a viscous flow. The equations for the boundary layer are obtained from the integral momentum relation [18], and they are solved jointly with the equations of the core flow, in which the channel is effectively represented as a function of the boundary-layer thickness. Numerical calculations are carried out for these simultaneous equations to investigate the effect of the Reynolds number and the configuration of the glottal channel, and the effective core flow velocity, flow separation point, and pressure distribution along the glottal channel are then obtained. The effect of flow asymmetry is examined for a large number of channel shapes. Numerical results are also compared with those obtained by one-dimensional IBL analysis [10] to quantitatively evaluate the applicability of the conventional one-dimensional assumption.

2. BOUNDARY-LAYER ANALYSIS OF GLOTTAL FLOW IN AN ASYMMETRICAL CHANNEL

On the basis of the IBL analysis [10,11,15,17], a method is presented in this section to analyze the behavior of glottal flow passing through an asymmetrical channel. For flow that has a high Reynolds number, the core flow region outside the boundary layer can be considered as inviscid, while the effect of air viscosity is apparent in the vicinity of the wall of the channel and in the wake. As such, the boundary-layer approximation permits a constitutive representation of the entire flow field. Besides the boundary-layer approximation, the glottal flow is thought to be quasi-steady and incompressible, since the typical Strouhal number is of the order of 10^{-2} and the flow velocity is sufficiently lower than the sound velocity with a Mach number less than 0.1 [9]. Our previous study [11] also indicates that the one-dimensional IBL analysis is accurate for a symmetrical glottal channel; however, for an asymmetrical channel, the flow velocities of the left and right walls can differ [13,14,19], indicating that the analysis of the boundary-layer and core flow should, at least, be performed in two dimensions.

The boundary-layer equations can numerically be solved using the Pohlhausen method [18]. When the Reynolds number is sufficiently high, the thickness of the boundary layer can to a first approximation be neglected, since it is inversely proportional to the square root of the Reynolds number. However, our numerical examinations revealed that the layer thickness is more than 10% of the total channel width at the flow separation point even for a Reynolds number of two or three thousand [11]. Because the boundary-layer thickness affects the effective size of the glottal channel, it should be taken into consideration for the analysis of the flow velocities. Inversely, a change in the core flow velocity affects the solution of the boundary-layer problem as indicated by the Kármán-Pohlhausen framework. This strongly suggests that the viscous (boundary layer) and inviscid (core flow) parts of the glottal flow interact with one another [17], and their governing equations should be combined to obtain a proper solution. In this study, the complex variable analysis technique is applied for the core flow owing to its incompressible, irrotational nature.

2.1. The Boundary-layer Equation

The momentum-integral equation of the boundary layer is expressed as

$$\frac{d}{dx}\{v^2\theta\} + \delta v \frac{d}{dx} v = \frac{\tau}{\rho} \tag{1}$$

for two-dimensional steady flow [18], where δ[cm] is the displacement thickness, θ[cm] is the momentum thickness, τ[g/cm·s^2] is the wall shear stress, and ρ[g/cm^3] is the density of the air. A curvilinear coordinate system is used, with the x-axis following the surface of the vocal fold. v[cm/s] is the velocity of the core flow along the outer edge of the boundary layer, giving the boundary condition of the equation. The characteristic quantities of the boundary layer, δ, θ, and τ, are functions of x. The flow velocity in the boundary layer has been integrated out in Eq. (1) and is implicitly related via the definition of these characteristic quantities. Continuity requires that the

internal velocity agrees with the core flow velocity at the outer edge of the boundary layer.

When a Hartree profile is assumed to represent the velocity profiles of the boundary-layer equation, Eq. (1) can be rewritten as [17]

$$\frac{\delta^2}{\nu}\frac{dv}{dx} = f_1(H) \tag{2}$$

and

$$v\frac{\delta}{\nu}\frac{d}{dx}\frac{\delta}{H} + \left(1+\frac{2}{H}\right)f_1(H) = Hf_2(H), \tag{3}$$

where H is the ratio of the displacement and momentum thicknesses ($H = \delta/\theta$) and ν[cm^2/s] is the kinematic viscosity. f_1 and f_2 are approximation functions given by Kalse *et al.* [17]:

$$f_1(H) = -2.4\{1 - \exp(0.43(2.59 - H))\} \tag{4}$$

and

$$f_2(H) = \frac{4}{H^2} - \frac{1}{H}. \tag{5}$$

These equations can be solved for the specified value of the core flow velocity, v, along the x axis. Additionally, the separation point of the boundary layer can be estimated by finding the x-axis position where the wall shear stress becomes zero. This indicates that $H = 4$ and $f_2 = 0$ at the separation point.

For an asymmetrical glottal channel, the boundary-layer equations should be solved independently for each vocal fold. We here denote quantities using the subscripts L and R, such as δ_L and δ_R for the left and right vocal folds. In the analysis of asymmetrical flow, there are six unknown variables, namely v_L, v_R, δ_L, δ_R, H_L, and H_R. Here, v_L, δ_L, and H_L are functions of the x_L axis following the surface of the left vocal fold (see Fig. 1). v_R, δ_R, and H_R, on the other hand, are functions of the x_R axis. As will be explained below, Eqs. (2) and (3) are combined with the equations giving the effective core flow velocity, and the resulting nonlinear simultaneous equations are solved to determine the values of the unknown variables.

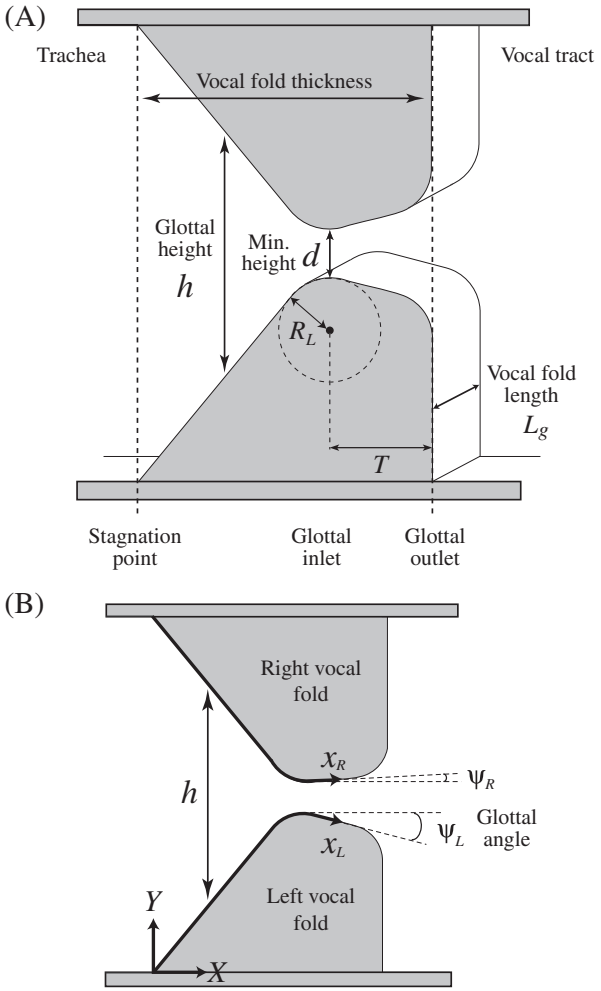

Fig. 1 The vocal fold shape is represented using the model proposed by Scherer *et al.* [13]. The model is mainly controlled by three parameters representing the minimum height of the channel (d) and the glottal angles (ψ_L and ψ_R). h represents the height of the channel. L_g is the length of the vocal fold and T is a fixed parameter. As shown in (B), the axes, x_L and x_R, are taken along the surface of each vocal fold for the boundary-layer analysis. On the other hand, the X and Y axes are used for the potential flow analysis of the core flow. The glottal angles are defined as the opening angle of the vocal fold relative to the direction of the X axis. The glottal height is the distance between both vocal folds measured in the direction of the Y axis. Therefore, h is a function of the X axis.

2.2. Equation of the Core Flow Velocity

Owing to the incompressible, inviscid, and irrotational nature, the velocity field of the core flow is governed by the Laplace equation $\nabla \cdot \boldsymbol{v} = \nabla^2\phi = 0$, where $\boldsymbol{v} = (v_X, v_Y)$ is the flow velocity and ϕ is the velocity potential. The two-dimensional potential flow is analyzed conveniently by applying complex variable theory [20]. Let $z = X + jY$ denote a complex argument, where X and Y are the axes of an orthogonal coordinate system as illustrated in Fig. 1(B). j is the imaginary unit. In addition, the complex potential function is defined as $f = \phi + j\varphi$, where ϕ is the velocity potential and φ is the stream function. It follows that $df/dz = v_X - jv_Y$, and the absolute flow velocity is $v = |df/dz|$.

As the complex potential function, $f = Uz$ for example represents uniform flow in the unbounded free field flowing in the direction of the real axis at a speed of U, since $df/dz = U$ and U is a real value ($v_X = U$ and $v_Y = 0$). This potential function is adapted to the bounded, actual configuration of the glottis employing conformal trans-

formation; i.e., the Schwartz-Christoffel formula [21]. In this technique, the flow region with the actual boundary shape is called the physical domain and that of the infinite strip the canonical domain. Let $z = X + jY$ and $\zeta = \xi + j\eta$ be complex arguments representing the coordinate systems of the physical and canonical domains, respectively. Additionally, g is the mapping function that connects the two domains according to $z = g(\zeta)$. The flow velocity in the physical domain is expressed as

$$v_X - jv_Y = \frac{df}{dz} = \frac{df}{d\zeta}\frac{d\zeta}{dz} = \frac{df}{d\zeta}\frac{1}{g'(\zeta)}, \tag{6}$$

where $g'(\zeta) = dz/d\zeta$. The potential function of the uniform flow in the canonical domain is expressed as $f(g(\zeta)) = V\zeta$, and it is used to represent the expiratory flow from the lungs. V is a constant related to the volume flow rate of the glottal flow such that $V = U_g/L_g$, where $U_g[\mathrm{cm}^3/\mathrm{s}]$ is the glottal volume flow rate and $L_g[\mathrm{cm}]$ is the length of the vocal folds. The flow velocity in the physical domain can then be rewritten as

$$v_X - jv_Y = \frac{V}{g'(\zeta)}. \tag{7}$$

To derive the mapping function, the shape of the glottal channel is first approximated by polygonal lines with N vertices (z_k, $k = 1, 2, \ldots, N$) in the physical domain, and the corresponding vertices ζ_k in the canonical domain are then determined. The mapping function for the infinite stripe is expressed following the Schwartz-Christoffel formula as [21]

$$g(\zeta) = C\int_0^{\zeta}\prod_{k=1}^{N}\left[\sinh\frac{\pi}{2}(\eta - \zeta_k)^{\alpha_k - 1}\right]d\eta, \tag{8}$$

where $\alpha_k\pi$ is the interior angle of the kth vertex in the physical domain. This equation is different in some aspects from its textbook definition [21]. First, the term $\exp[\frac{\pi}{2}(\alpha_- - \alpha_+)\zeta]$ included in the original equation [Eq. (4.4) on page 46 of the textbook] is omitted, since the divergence angles α_- and α_+ at the two ends of the canonical domain (infinite strip) are equal. Second, the constant term A included in the original equation is set to zero, so that the origin of the ζ axis is mapped to that of the z axis. The scaling factor C is set to the channel height at the stagnation point.

The positions of the vertices in the physical domain should be specified by the user, but those of the corresponding vertices in the canonical domain are not known. If the vertex alignment is determined for both domains, the mapping function requires numerical integration. In addition, the flow analysis procedure requires the inverse mapping: $\zeta = g^{-1}(z)$. These numerical issues can be solved using the techniques explained in the textbook [21].

2.3. The IBL Problem for an Asymmetrical Channel

Next, we formulate the IBL problem and show how it is solved numerically. If the development of the boundary layer is not considered, the flow velocity along the surface of the left or right vocal fold, x, can be obtained from Eq. (7) as

$$v_s(x) = \left|\frac{V}{g'(\zeta)}\right| \quad (\zeta = \zeta_s(x)), \tag{9}$$

where $\zeta_s(x)$ represents the glottal shape in the canonical domain: a straight channel. If $z(x)$ is a complex variable in the physical domain along the glottal surface, $\zeta_s(x)$ is determined as $\zeta_s(x) = g^{-1}(z(x))$, where $\zeta = g^{-1}(z)$ is the inverse mapping of Eq. (8). Following our foregoing study on the symmetrical glottal channel [11], we suppose that the effective core flow velocity, v, is given by the sum of two components:

$$v = v_s + v_\delta \tag{10}$$

and

$$v_\delta = v_s\frac{\delta_L + \delta_R}{h - (\delta_L + \delta_R)}, \tag{11}$$

where $\delta_L + \delta_R$ is the total layer thickness of both vocal folds. The second term, v_δ, represents the change in the velocity due to the development of the boundary layer.

Finally, the IBL problem for an asymmetrical channel is obtained as a set of six nonlinear simultaneous equations by considering Eqs. (2), (3), and (11) for both vocal folds:

$$\frac{\delta_L^2}{\nu}\frac{dv_L}{dx_L} = f_1(H_L), \tag{12}$$

$$\frac{\delta_R^2}{\nu}\frac{dv_R}{dx_R} = f_1(H_R), \tag{13}$$

$$v_L\frac{\delta_L}{\nu}\frac{d}{dx_L}\frac{\delta_L}{H_L} + \left(1 + \frac{2}{H_L}\right)f_1(H_L) = H_L f_2(H_L), \tag{14}$$

$$v_R\frac{\delta_R}{\nu}\frac{d}{dx_R}\frac{\delta_R}{H_R} + \left(1 + \frac{2}{H_R}\right)f_1(H_R) = H_R f_2(H_R), \tag{15}$$

$$v_{\delta L} = v_{sL}\frac{\delta_L + \delta_R}{h - (\delta_L + \delta_R)}, \tag{16}$$

and

$$v_{\delta R} = v_{sR}\frac{\delta_L + \delta_R}{h - (\delta_L + \delta_R)}, \tag{17}$$

with constraints

$$v_L = v_{sL} + v_{\delta L} \tag{18}$$

and

$$v_R = v_{sR} + v_{\delta R}. \tag{19}$$

The unknown variables in these equations are $v_{\delta L}$, $v_{\delta R}$, δ_L,

δ_R, H_L, and H_R. The boundary-layer equations, Eqs. (12) through (15), are separated for each vocal fold, while the core flow relations, Eqs. (16) and (17), are coupled by the displacement thicknesses, δ_L and δ_R.

The procedure for solving this interactive flow analysis problem is as follows. For prescribed values of the vocal fold shapes (x_L and x_R), channel height (h), and the volume flow rate (U_g), the potential flow analysis is first performed to determine the nominal flow velocities, v_{sL} and v_{sR}. Here, node points are aligned along the x_L and x_R axes such that $\{x_{L0}, x_{L1}, x_{L2}, x_{L3}, \ldots, x_{Li}, \ldots\}$ and $\{x_{R0}, x_{R1}, x_{R2}, x_{R3}, \ldots, x_{Ri}, \ldots\}$. x_{L0} and x_{R0} are the stagnation points [see Fig. 1(A)], and the indices are assigned to the downstream direction. The values of v_{sL} and v_{sR} are then calculated using Eq. (9) for each node point.

Next, Eqs. (12) through (17) are solved employing downstream marching as in the previous studies [10,11]. At the origin of the x_L and x_R axes, the initial values are set to $v_{\delta L}(0) = 0$, $v_{\delta R}(0) = 0$, $\delta_L(0) = 0$, $\delta_R(0) = 0$, $H_L(0) = 2.216$, and $H_R(0) = 2.216$, because x_{L0} and x_{R0} are the flow stagnation points (see page 197 of the literature [18]). Starting from these given values, the solutions are obtained repeatedly at each node point, x_{Li} and x_{Ri} ($i = 1, 2, 3, \ldots$), in the downstream direction.

Here, the functions to be zeroed are defined as

$$F_1(i) = \frac{\delta_L(x_{Li})^2}{\nu} \frac{v(x_{Li}) - v(x_{Li-1})}{|x_{Li} - x_{Li-1}|} - f_1(H_L(x_{Li})), \tag{20}$$

$$F_2(i) = \frac{\delta_L(x_{Ri})^2}{\nu} \frac{v(x_{Ri}) - v(x_{Ri-1})}{|x_{Ri} - x_{Ri-1}|} - f_1(H_R(x_{Ri})), \tag{21}$$

$$\begin{aligned} F_3(i) = {} & v_L(x_{Li}) \frac{\delta_L(x_{Li})}{\nu} \left(\frac{\delta_L(x_{Li})}{H(x_{Li})} - \frac{\delta_L(x_{Li-1})}{H(x_{Li-1})} \right) \frac{1}{|x_{Li} - x_{Li-1}|} \\ & + \left(1 + \frac{2}{H_L(x_{Li})} \right) f_1(H_L(x_{Li})) \\ & - H_L(x_{Li}) f_2(H_L(x_{Li})), \end{aligned} \tag{22}$$

$$\begin{aligned} F_4(i) = {} & v_R(x_{Ri}) \frac{\delta_R(x_{Ri})}{\nu} \left(\frac{\delta_R(x_{Ri})}{H(x_{Ri})} - \frac{\delta_R(x_{Ri-1})}{H(x_{Ri-1})} \right) \frac{1}{|x_{Ri} - x_{Ri-1}|} \\ & + \left(1 + \frac{2}{H_R(x_{Ri})} \right) f_1(H_R(x_{Ri})) \\ & - H_R(x_{Ri}) f_2(H_R(x_{Ri})), \end{aligned} \tag{23}$$

$$F_5(i) = v_{\delta L}(x_{Li}) - v_{sL}(x_{Li}) \frac{\delta_L(x_{Li}) + \delta_R(x_{Ri})}{h(i) - \delta_L(x_{Li}) - \delta_R(x_{Ri})}, \tag{24}$$

and

$$F_6(i) = v_{\delta R}(x_{Ri}) - v_{sR}(x_{Ri}) \frac{\delta_L(x_{Li}) + \delta_R(x_{Ri})}{h(i) - \delta_L(x_{Li}) - \delta_R(x_{Ri})}. \tag{25}$$

The values of $v_{\delta L}(x_{Li})$, $v_{\delta R}(x_{Ri})$, $\delta_L(x_{Li})$, $\delta_R(x_{Ri})$, $H_L(x_{Li})$, and $H_R(x_{Ri})$ are then determined so as to minimize the values of F_1 through F_6 simultaneously, for $i = 1, 2, 3, \ldots$, until the exit of the glottis. This optimization can be performed employing, for example, the Newton-Raphson method [10,11].

Note that differential operations are replaced by finite differences in the cost functions. x_{Li-1} and x_{Ri-1} are the upstream points at which the value of every variable is already determined. $|x_{Li} - x_{Li-1}|$ and $|x_{Ri} - x_{Ri-1}|$ are the distances of succeeding node points. Additionally, the channel height, h, is included in F_5 and F_6, requiring that the ith node points, x_{Li} and x_{Ri}, determine the edges of the ith channel height, $h(i)$.

2.4. Estimation of the Volume Flow Rate for the Specific Subglottal Pressure

In our previous studies [10,11], the numerical computation was successfully carried out and the IBL problem was solved for both one- and two-dimensional flows in symmetrical glottal channels. In addition, through a preliminary examination, we ensured that the new analysis method presented in this article can provide proper results if the channel shape is symmetrical. If the channel is asymmetrical, however, the numerical results seem to be inaccurate near the point of flow separation; this may related to the problem of Goldstein's singularity [22], but we could not determine the true cause. Because the volume flow rate is determined from the glottal area at the flow separation point [10], estimation of the flow rate is impossible owing to the instability.

To solve the problem, we take notice of the flow measurement data obtained by Scherer *et al.* [13,14] and Shinwari *et al.* [19] for oblique glottal channels; i.e., the pressure difference between the two vocal folds is apparent near the entrance of the glottis, but less significant downstream. From the observation, we here assume that the flow behavior along the surface of the left and right vocal folds is equivalent downstream of the glottal entrance, and the flow behavior can be treated as being one-dimensional. This means that the flow analysis is first performed in two dimensions, as explained in this section, from the stagnation point to a certain point on the X-axis downstream of the glottal entrance, and then, the analysis method is switched to one dimension until the flow separation point. The one-dimensional analysis [10] requires the initial values of the core flow velocity, displacement thickness of the boundary layer, and the shape factor at the switching point to employ the downstream marching technique, but they are conveniently obtained from the result of the two-dimensional analysis at that point. The switching point can be determined, for example, as the point on the X-axis where the nominal velocities of the two vocal folds (v_{sL} and v_{sR}) agree.

After the flow separation point, X_s, is estimated by the one-dimensional IBL analysis, the volume flow rate, U_g, is determined from Bernoulli's law as

$$U_g = S\sqrt{\frac{2P_0}{\rho}}, \tag{26}$$

where P_0 is the specified subglottal pressure. S is the effective sectional area of the glottis at the flow separation point, $S = L_g\{h(X_s) - 2\delta(X_s)\}$, where δ is the common displacement thickness of the two vocal folds.

3. NUMERICAL RESULTS

3.1. Experimental Conditions

This section presents the results of numerical investigations. The shape of the flow channel is controlled using the vocal fold model shown in Fig. 1 [13]. The model has parameters representing the minimum glottal height, d[cm], and the tilt angles of the two vocal folds, ψ_L and ψ_R[deg]. Other parameters of the model are set as $T = 0.3$ cm and $L_g = 1.2$ cm. The height of the trachea and the vocal tract tubes is 1.73 cm. To approximate the glottal shape and derive the conformal mapping, 20 vertices are placed along each curved section of the vocal fold model with equal intervals, and are connected with line segments. Vertices are also placed at the stagnation point and the end point of the vocal fold at the glottal outlet. The node points, x_{Li} and x_{Ri}, for solving the IBL problem are set so that the distance between the adjacent nodes is approximately 10^{-3} cm. The air density is $\rho = 1.184\,\mathrm{kg/m^3}$, and the dynamic viscous coefficient is $\mu = 0.0182 \times 10^{-3}$ Pa·s.

3.2. Estimation of the Volume Flow Rate

Estimation results are plotted in Figs. 2 and 3 for various glottal shapes. The subglottal pressure, P_0, was set to 10 cmH_2O (about 980.7 Pa) and the minimum glottal height, d, to 0.08 mm in this experiment. The angle of the left vocal fold, ψ_L, was varied as $-10°$, $-5°$, $0°$, $5°$, and $10°$. The angle of the right vocal fold, ψ_R, was changed from $-10°$ to $10°$ at $1°$ intervals for each value of ψ_L.

Figure 2 plots the shape of the vocal folds for 35 combinations of the angle parameters, ψ_L and ψ_R; the value of ψ_L is fixed in each row, while that of ψ_R is fixed in each column. Boxes drawn with the thick lines indicate the glottal channel having a uniform configuration, indicating that the two vocal folds are parallel. The glottal shape is convergent to the left of the uniform configuration, and the figure shows that the flow separation point indicated by the arrows is near the glottal exit for that shape. As the angle of the right vocal fold increases from $-10°$ to $10°$ and the glottis takes a divergent shape, the separation point tends to move gradually in the upstream direction. As explained in subsection 2.4, the volume flow rate and flow separation point were estimated from the one-dimensional IBL analysis. Therefore, the separation point for the left vocal fold and that for the right fold are located at the same point on the X-axis.

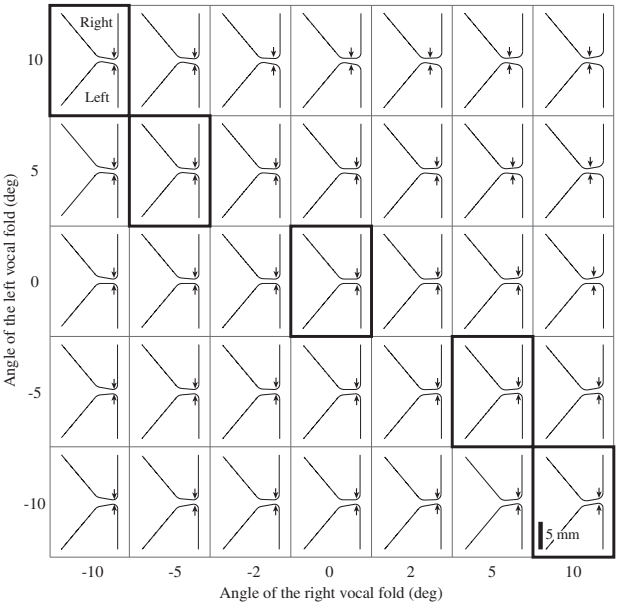

Fig. 2 The shape of the left and right vocal folds for the angles of $\psi_L = -10°$, $-5°$, $0°$, $5°$, $10°$ and $\psi_R = -10°$, $-5°$, $-2°$, $0°$, $2°$, $5°$, $10°$. When the absolute values of the two angle parameters are equivalent and the signs are opposite, the glottis forms a uniform channel, as indicated by boxes with the thick lines. For each row (ψ_L is constant), the vocal fold shape is convergent to the left of this uniform shape and divergent to the right. Arrows attached to the vocal folds indicate the estimated point of flow separation. The subglottal pressure was 10 cmH_2O and the minimum glottal height was 0.08 cm.

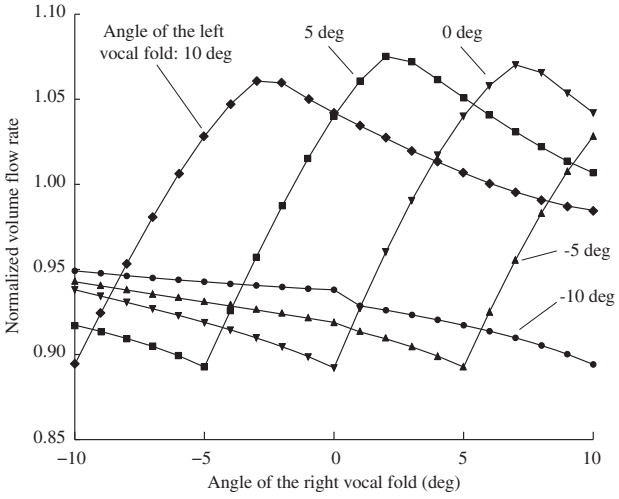

Fig. 3 Estimated volume flow rate normalized by a specific value ($dL_g\sqrt{2P_0/\rho}$). The subglottal pressure was 10 cmH_2O and the minimum glottal height was 0.08 cm.

The estimated volume flow rate was normalized by a specific flow value, $dL_g\sqrt{2P_0/\rho}(= 390.7\,\mathrm{cm^3/s})$, which corresponds to the Reynolds number of about 2,100, and the results are plotted in Fig. 3 as a function of the angle

parameter, ψ_R. The total number of glottal configurations is 105, but 20 shapes are the reverse versions of their counterparts for which the angles of left and right vocal folds are switched. Note that the volume flow rate is equivalent when the glottal configuration is reversed.

Irrespective of the constant subglottal pressure, the flow rate varies as the glottal shape changes. For the conditions $\psi_L = 0°$, $5°$, and $10°$, the peak of the normalized flow rate is at $\psi_R = 7°$, $2°$, and $-3°$, respectively. The glottal shape is divergent for these angle conditions, as shown in Fig. 2. Figure 3 shows that the flow rate is a minimum when the angle condition is $(\psi_L, \psi_R) = (-10, 10)$, $(-5, 5)$, $(0, 0)$, $(5, -5)$, or $(10, -10)$ and the glottis takes a uniform configuration.

To interpret the results of Fig. 3, note that the flow rate is in proportion to the glottal area at the separation point, as described by Eq. (26). For the uniform and convergent glottal shapes, the flow separates near the point at which the glottal height is a minimum. For the divergent shape, on the other hand, the glottal height is a minimum near the glottal entry and the flow separation point is near the exit; thus, the glottal area at the separation point and consequently the flow rate increase. The increase and decrease in the volume flow rate can thus be explained by the movable nature of the flow separation point, which strongly depends on the channel configuration. In Fig. 3, the flow rate is a maximum when the sum of ψ_L and ψ_R is $7°$, but this angle may depend on the subglottal pressure or the minimum glottal height.

3.3. Profiles of the Effective Velocity and Pressure along the Vocal Folds

The profile of the effective core flow velocity and the aerodynamic pressure were computed for the left vocal fold angle of $0°$ and the right vocal fold angle of $-10°$, $0°$, and $7°$ forming convergent, uniform, and divergent glottal channels, respectively, as shown in Fig. 4. The subglottal pressure was $10\,cmH_2O$ and the minimum glottal height was 0.08 cm, and they were the same as those for Fig. 3. The estimated volume flow rate was $366.5\,cm^3/s$ corresponding to a Reynolds number of about 1987 for $\psi_R = -10°$, $348.6\,cm^3/s$ corresponding to a Reynolds number of 1,890 for $\psi_R = 0°$, and $418.1\,cm^3/s$ corresponding to a Reynolds number of 2,267 for $\psi_R = 7°$.

For each angle condition, the second and third plots from the top in Fig. 4 show the velocity profiles along the surface of each vocal fold. The thick lines show the effective velocities, v_L and v_R, as functions of the X-axis, and the thin lines show the nominal velocities, v_{sL} and v_{sR}. Note that the nominal velocities were computed for the entire glottal region, but the effective velocities were obtained for the region upstream of the separation point indicated by the arrows in the top plot of the figure. The

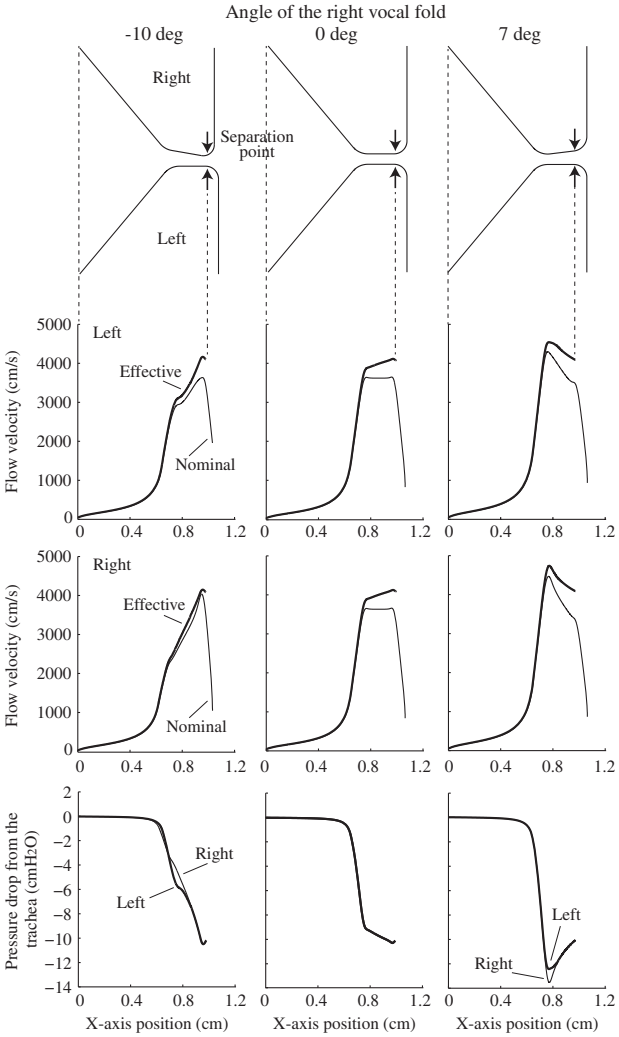

Fig. 4 From top to bottom, the plots show the glottal shape, velocity along the surface of the left vocal fold, velocity along the right vocal fold, and pressure distribution for both vocal folds. The angle of the left vocal fold was fixed at $0°$, while that of the right vocal fold was varied as $-10°$, $0°$, and $7°$, respectively. The effective velocities, v_L and v_R in Eqs. (18) and (19), are drawn with thick lines, and the nominal velocities, v_{sL} and v_{sR}, with thin lines. The subglottal pressure was $10\,cmH_2O$ and the minimum glottal height was 0.08 cm.

effective velocity is in general greater than the nominal one, because the volume flow rate is predetermined from the lung pressure and the channel height in essence decreases owing to the development of the boundary layer [10,11]. It can be observed from the figure that the difference between the effective and nominal velocities is prominent for each glottal shape just upstream of the separation point.

When the channel is convergent ($\psi_R = -10°$), the velocity is a maximum near the separation point. The difference in the nominal velocity is considerable between the left and right vocal folds near this point; however, the

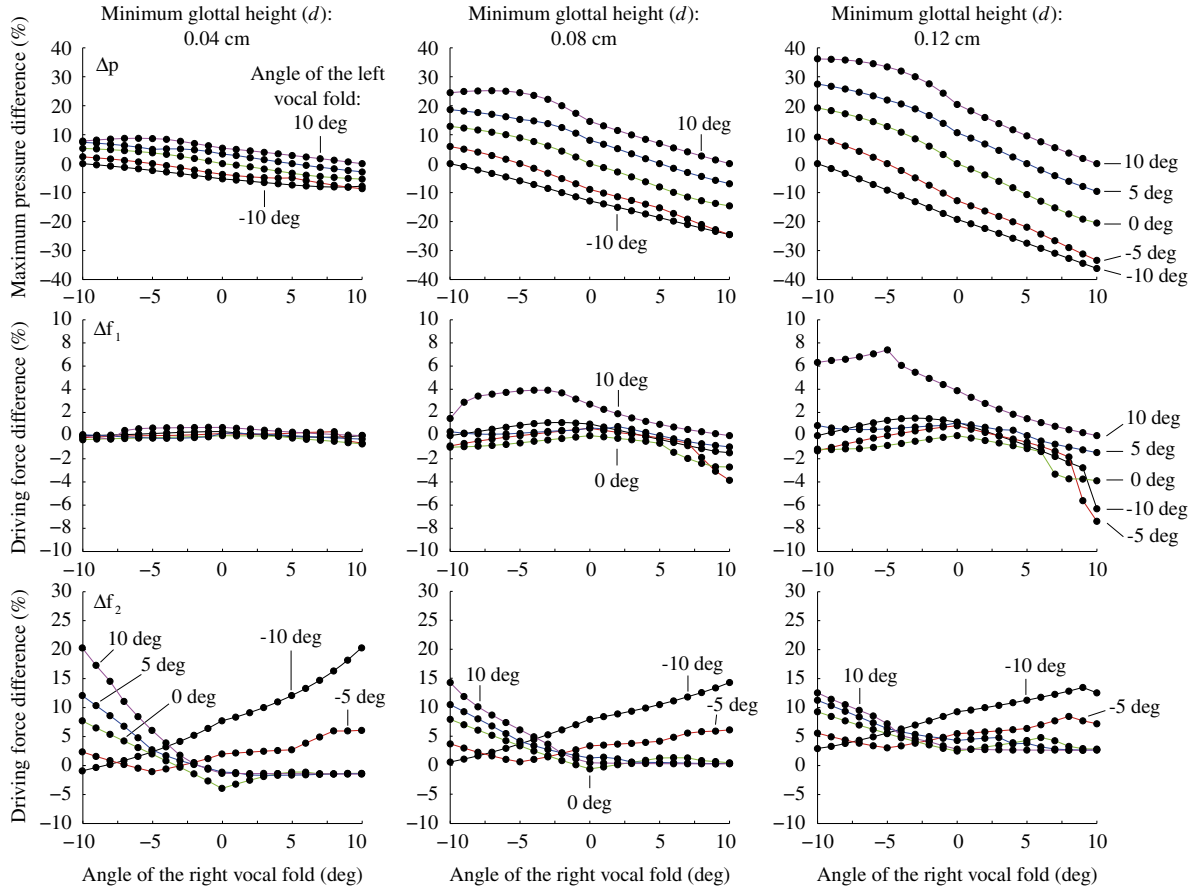

Fig. 5 The maximum pressure difference between the two vocal folds (top), the difference in the driving forces between the two vocal folds (middle), and the difference in the driving forces calculated in the one- and two-dimensional flow analyses (bottom). The maximum pressure difference was normalized by the subglottal pressure. The driving force difference was normalized by a specific value, $0.3L_gP_0$ [dyn], where 0.3 cm is a representable value of the vocal fold thickness. The subglottal pressure, P_0, was 10 cmH_2O.

difference in the effective velocity is not so large. This suggests that the development of the boundary layer decreases the velocity difference for the two vocal folds arising from channel asymmetry. As a result, the flow behavior approaches one-dimensional behavior.

The effect is also seen in the pressure profiles plotted at the bottom of Fig. 4. Here, the pressure drop from the trachea was calculated using the effective velocity and Bernoulli's law as $p_L = -0.5\rho v_L^2$ and $p_R = -0.5\rho v_R^2$ for the left and right vocal folds. For each glottal shape, the pressure values of the two vocal folds are almost the same in the vicinity of the flow separation point. For the convergent and divergent shapes, the difference is apparent only for the region near the glottal entrance ($X \approx 0.8$ cm).

In addition, the maximum pressure drop of the divergent shape is about -12.4 cmH_2O for the left and -13.5 cmH_2O for the right. The absolute values are obviously greater than the subglottal pressure (10 cmH_2O). Although the glottal configuration is not exactly the same, Scherer *et al.* [13] showed, through aerodynamic measurement, a similar prominent pressure drop for the glottis with an oblique angle of 15° and included angle of 10°.

3.4. Driving Force of the Vocal Folds

Finally, we examine the maximum of the difference between the two pressure values, p_L and p_R, determined from the flow velocity along the vocal folds and plotted in Fig. 4. These pressure values were also numerically integrated along the surface of the vocal folds to estimate their driving forces and degree of imbalance due to channel asymmetry. The driving force was also calculated in one-dimensional flow analysis [10] and the estimation was compared with that of two-dimensional analysis.

The results of these three types of investigations are presented at the top, middle, and bottom of Fig. 5, respectively. The subglottal pressure, P_0, was set to 10 cmH_2O. The minimum glottal height, d, was varied as 0.04, 0.08, and 0.12 cm as shown at the left, center, and right of the figure. The horizontal axis gives the angle of the right vocal fold, ψ_R. The angle of the left vocal fold, ψ_L, was varied as $-10°$, $-5°$, $0°$, $5°$, and $10°$. The total

number of glottal configurations is 105 for each glottal height, but 20 shapes are the reverse versions of their counterparts. When the glottal configuration is reversed, the velocity and pressure profiles of the two vocal folds are also reversed, indicating that the sign of the maximum pressure difference, Δp, and the sign of the driving force difference, Δf_1, are changed in the following.

The pressure values, p_L and p_R, were first computed as a function of the X-axis for each combination of the angles ψ_L and ψ_R. The maximum difference was then obtained as a normalized value:

$$\Delta p = \frac{p_R(X_{max}) - p_L(X_{max})}{P_0}, \tag{27}$$

where X_{max} is the position at which the absolute difference $|p_R(X) - p_L(X)|$ is a maximum. If Δp is small, the pressure difference between the two vocal folds is small, and hence, the flow behavior in the glottis can be regarded as being one-dimensional. Note that Δp is zero if $\psi_L = \psi_R$ holds and the channel is symmetrical.

When the minimum glottal height is 0.04 cm, the maximum pressure difference is within $\pm 10\%$ of the subglottal pressure, indicating that the flow behavior is likely to be one-dimensional. The maximum difference increases noticeably as the minimum glottal height increases; the difference is approximately three times as much when d is 0.08 mm and four times as much when d is 0.12 mm. Here, it is noteworthy that the maximum pressure difference usually occurs in the vicinity of the glottal entrance as shown in Fig. 4. In the other part of the glottis, the pressure difference of the two vocal folds may be negligible. Therefore, the pressure values were integrated along the vocal fold surface to compare the driving forces of the two vocal folds.

The difference in the driving forces is plotted in the middle of the figure as

$$\Delta f_1 = \frac{f_R - f_L}{0.3 L_g P_0}, \tag{28}$$

where 0.3 cm is a representative value of the vocal fold thickness. f_L and f_R are the forces of the left and right vocal folds, respectively, computed such that

$$f_L = L_g \int_0^{x_{sep}} p_L(x_L) dx_L, \tag{29}$$

where x_{sep} is the flow separation point along the surface of the vocal fold. As a result, the difference is within $\pm 1\%$ when the minimum glottal height is 0.04 cm. The difference increases as the minimum glottal height increases: Δf_1 is within $\pm 4\%$ when d is 0.08 cm and within $\pm 8\%$ when d is 0.12 cm. However, if the range of the glottal angle is smaller such that $|\psi_L| \leq 5^\circ$ and $|\psi_R| \leq 5^\circ$, Δf_1 is within $\pm 2\%$ even when d is 0.12 cm, meaning that the two vocal folds are equally driven in the presence of glottal asymmetry.

One-dimensional IBL analysis [10,17] was also carried out, and the driving force was calculated as

$$f_1 = L_g \int_0^{x_{sep}} p_1(X) dX, \tag{30}$$

where p_1 is the one-dimensional pressure distribution. Note that the glottal height, $h(X)$ in Fig. 1, was used to specify the glottal shape in this analysis. The difference in the driving force is plotted at the bottom of the figure using a relative value

$$\Delta f_2 = \frac{1}{2} \frac{(f_1 - f_L) + (f_1 - f_R)}{0.3 L_g P_0}. \tag{31}$$

Near the surface of the vocal folds, the flow stream line is curved in general following the glottal shape. This two-dimensional effect is ignored in the one-dimensional analysis, and as a result, the estimated flow velocity is lower than the velocity estimated in two-dimensional analysis. The decrease in the flow velocity inversely increases the estimated value of the pressure, and hence the driving force. This is the reason why Δf_2 tends to be positive, indicating that $f_1 > f_L$ and $f_1 > f_R$. From the figure, the difference seems to increase as the absolute values of the vocal fold angles increase. Δf_2 is especially considerable when ψ_L is -10° and ψ_R is 10° or ψ_L is 10° and ψ_R is -10°, producing a slanted, uniform glottal shape.

The results for Δf_1 and Δf_2 shown in Fig. 5 were reconsidered in Fig. 6 by taking the average of their absolute values, $|\Delta f_1|$ and $|\Delta f_2|$. The condition of the vocal fold angles, $\Delta\psi = \psi_L - \psi_R$, was set such that $|\Delta\psi| \leq 5^\circ$ in (a), $|\Delta\psi| \leq 10^\circ$ in (b), $|\Delta\psi| \leq 15^\circ$ in (c), and $|\Delta\psi| \leq 20^\circ$ in (d). The figure indicates that $|\Delta f_1|$ increases as $\Delta\psi$ increases or d increases, but it is less than 2% on average even when d is 0.12 cm. On the other hand, $|\Delta f_2|$ is almost the same when d is 0.04 or 0.08 cm, and the total average plotted in (d) is about 4%. When d is 0.12 cm, $|\Delta f_2|$ increases and the total average in (d) is about 6%. These data are the expected errors when the flow behavior is analyzed in one dimension instead of using the precise, but complicated, two-dimensional analysis method.

4. SUMMARY AND CONCLUSIONS

The flow separation framework has been widely used to construct one-dimensional models of the glottal flow [2,9,10]. The analysis method based on the boundary-layer assumption has been further extended to two dimensions [11], but is still limited to symmetrical flows that are typical of regular phonation. This paper presented a method for analyzing the behavior of flow passing through an asymmetrical glottal channel which assumes the formation of a thin boundary layer near the glottal wall and the

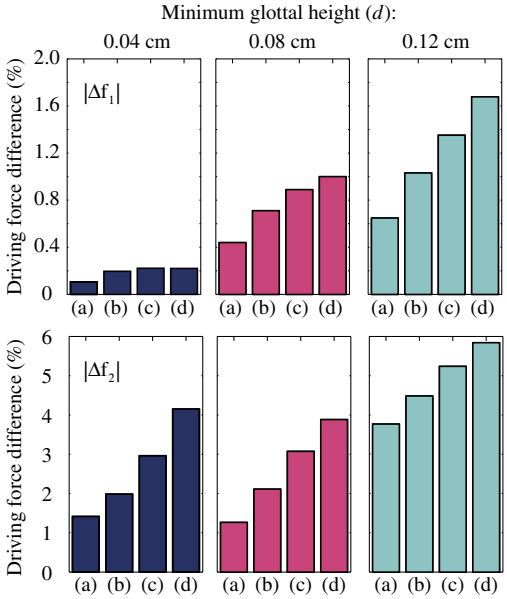

Fig. 6 Mean absolute value of Δf_1 and Δf_2 calculated by considering the difference in the angles, $\Delta\psi = \psi_L - \psi_R$. In (a), the mean was obtained using data samples for which $|\Delta\psi| \leq 5^\circ$ including the symmetrical case, $\psi_L = \psi_R$. In (b), (c), and (d), the means were respectively calculated for samples satisfying the conditions $|\Delta\psi| \leq 10^\circ$, $|\Delta\psi| \leq 15^\circ$, and $|\Delta\psi| \leq 20^\circ$. The number of samples was 45 in (a), 75 in (b), 95 in (c), and 105 in (d). All data samples were included in (d).

interaction between the boundary layer and the core flow. The core flow velocity was estimated through potential flow analysis [20,21], while the characteristic quantities of the boundary layer were determined by solving the integral momentum relation on the basis of the similarity of the velocity profiles inside the layer [18].

Several numerical experiments were conducted to reveal the effect of channel asymmetry on the glottal flow, such as the volume flow rate, effective flow velocity, pressure distribution, driving force of the vocal fold, and flow separation point. The shape of the glottal channel was determined by the angle parameter of each vocal fold and the minimum height of the glottis, and 315 configurations in total were used for the analysis.

First, numerical results showed, irrespective of the constant minimum glottal height, that the volume flow rate of glottal flow depends on the angle of the vocal folds because of the movable nature of the flow separation point. The flow rate tends to increase when the glottal shape is divergent, while it tends to decrease when the glottis forms a uniform or convergent configuration. The other important finding is that the development of the boundary layer reduces the effect of geometrical asymmetry of the glottal channel, even when the nominal flow velocity differs along each vocal fold owing to the geometrical asymmetry, and the difference in the effective velocity decreases when considering the thickness of the boundary layer. This implies that the flow behavior in an asymmetrical glottis can be analyzed well using conventional one-dimensional methods [9,10]. The estimation results obtained using the two analysis methods were therefore compared in a subsequent experiment in terms of the driving force of the vocal fold.

Next, the aerodynamic imbalance was investigated in terms of the maximum difference in the pressure distribution along the surfaces of the two vocal folds. This pressure difference increases as the difference in the glottal angles increases or the height of the glottis increases: the maximum difference is about 40% of the subglottal pressure when the glottal height is 0.12 cm and the difference in angle is 20 degrees. A further experiment was conducted by integrating the pressure distribution and estimating the driving force of the vocal fold. We found that the difference in the driving force is much smaller being less than 2% on average even when the glottal minimum height is 0.12 cm. When the driving force was estimated through one-dimensional analysis [10], on the other hand, the error between the one- and two-dimensional analysis methods was found to be about 6% on average, but the error strongly depended on the glottal height and the angle difference between the two vocal folds.

Employing the proposed analysis method, the computational cost for solving the boundary-layer equations is only twice that in the case of the one-dimensional method, but the computational method of the core flow velocity is much more complicated and the cost is much greater. To determine whether the error in the one-dimensional analysis is significant and whether the one-dimensional analysis is still effective for asymmetrical flows, further study will be carried out for the dynamic simulation of phonation by combining a mechanical model of the vocal fold with the proposed flow analysis method.

ACKNOWLEDGEMENT

This research was partly supported by a Grant-in-Aid for Scientific Research from the Japan Society for the Promotion of Science (Grant No. 23300071).

REFERENCES

[1] Jw. van den Berg, "Myoelastic-aerodynamic theory of voice production," *J. Speech Hear. Res.*, **1**, 227–244 (1958).
[2] K. Ishizaka and J. L. Flanagan, "Synthesis of voiced sounds from a two-mass model of the vocal cords," *Bell Syst. Tech. J.*, **51**, 1233–1268 (1972).
[3] I. R. Titze, "Nonlinear source-filter coupling in phonation: Theory," *J. Acoust. Soc. Am.*, **123**, 2733–2749 (2008).
[4] K. Ishizaka and N. Isshiki, "Computer simulation of pathological vocal-cord vibration," *J. Acoust. Soc. Am.*, **60**, 1193–1198 (1976).
[5] D. Wong, M. R. Ito, N. B. Cox and I. R. Titze, "Observation of

perturbations in a lumped-element model of the vocal folds with application to some pathological cases," *J. Acoust. Soc. Am.*, **89**, 383–394 (1991).

[6] I. Steinecke and H. Herzel, "Bifurcations in an asymmetric vocal-fold model," *J. Acoust. Soc. Am.*, **97**, 1874–1884 (1995).

[7] P. Mergell, H. Herzel and I. R. Titze, "Irregular vocal-fold vibration—High-speed observation and modeling," *J. Acoust. Soc. Am.*, **108**, 2996–3002 (2000).

[8] Y. Zhang and J. J. Jiang, "Chaotic vibrations of a vocal fold model with a unilateral polyp," *J. Acoust. Soc. Am.*, **115**, 1266–1269 (2004).

[9] X. Pelorson, A. Hirschberg, R. R. van Hassel, A. P. J. Wijnands and Y. Auregan, "Theoretical and experimental study of quasisteady-flow separation within the glottis during phonation. Application to a modified two-mass model," *J. Acoust. Soc. Am.*, **96**, 3416–3431 (1994).

[10] T. Kaburagi, "On the viscous-inviscid interaction of the flow passing through the glottis," *Acoust. Sci. & Tech.*, **29**, 167–175 (2008).

[11] T. Kaburagi and Y. Tanabe, "Low-dimensional models of the glottal flow incorporating viscous-inviscid interaction," *J. Acoust. Soc. Am.*, **125**, 391–404 (2009).

[12] C. Tao, Y. Zhang, D. G. Hottinger and J. J. Jiang, "Asymmetric airflow and vibration induced by the Coanda effect in a symmetric model of the vocal folds," *J. Acoust. Soc. Am.*, **122**, 2270–2278 (2007).

[13] R. C. Scherer, D. Shinwari, K. J. De Witt, C. Zhang, B. R. Kucinschi and A. A. Afjeh, "Intraglottal pressure profiles for a symmetric and oblique glottis with a divergence angle of 10 degrees," *J. Acoust. Soc. Am.*, **109**, 1616–1630 (2001).

[14] R. C. Scherer, D. Shinwari, K. J. De Witt, C. Zhang, B. R. Kucinschi and A. A. Afjeh, "Intraglottal pressure profiles for a symmetric and oblique glottis with a uniform duct," *J. Acoust. Soc. Am.*, **112**, 1253–1256 (2002).

[15] T. Kaburagi, "Voice production model integrating boundary-layer analysis of glottal flow and source-filter coupling," *J. Acoust. Soc. Am.*, **129**, 1554–1567 (2011).

[16] P. Y. Lagrée, A. Van Hirtum and X. Pelorson, "Asymmetrical effects in a 2D stenosis," *Eur. J. Mech. B/Fluids*, **26**, 83–92 (2007).

[17] S. G. C. Kalse, H. Bijl and B. W. van Oudheusden, "A one-dimensional viscous-inviscid strong interaction model for flow in indented channels with separation and reattachment," *ASME J. Biomech. Eng.*, **125**, 355–362 (2003).

[18] H. Schlichting and K. Gersten, *Boundary-Layer Theory*, 8th ed. (Springer Verlag, New York, 1999).

[19] D. Shinwari, R. C. Scherer, K. J. De Witt and A. A. Afjeh, "Flow visualization and pressure distributions in a model of the glottis with a symmetric and oblique divergent angle of 10 degrees," *J. Acoust. Soc. Am.*, **113**, 487–497 (2003).

[20] G. K. Batchelor, *An Introduction to Fluid Dynamics* (Cambridge University Press, New York, 2000).

[21] T. A. Driscoll and L. N. Trefethen, *Schwartz-Christoffel Mapping* (Cambridge University Press, New York, 2002).

[22] S. Goldstein, "On laminar boundary layer flow near a point of separation," *Q. J. Mech. Appl. Math.*, **1**, 43–69 (1948).